Collective Electronic Motion in a Metallic Slab*

K. L. KLIEWER AND RONALD FUCHS
Institute for Atomic Research and Department of Physics, Iowa State University, Ames, Iowa
(Received 1 August 1966)

The virtual modes are obtained for a free-electron-gas model of a metallic slab. These modes, excitations of the crystal which couple to radiative fields outside the slab, correspond to a mixture of collective electron motion and photons. It is shown that a knowledge of the virtual modes leads to a complete understanding of those aspects of the optical properties related to the long-wavelength collective behavior of the electrons. In particular, the existence of radiative surface modes is established. These modes markedly affect the low-frequency optical properties. Manifestations of the virtual modes in experimental situations other than optical investigations are discussed. The dispersion of the ordinary nonradiative surface plasmons at long wavelengths is also calculated using the same general technique. The result is in accord with a previous calculation.

I. INTRODUCTION

IN two recent papers,[1,2] we presented a method for determining the frequencies of the long-wavelength collective excitations of an ionic crystal slab oriented as indicated in Fig. 1. These excitations, resulting from the coupling of photon and phonon fields,[3] were shown to be of various types. In the nonradiative region[1] ($\omega<k_xc$)[4] there occur modes localized roughly at the surfaces (surface modes), and modes which have an oscillatory spatial dependence in the slab; for both types the fields have an exponential spatial decay outside the slab. In the radiative range[2] ($\omega>k_xc$), it was shown that the excitations can be described by virtual modes, which correspond to fields decaying exponentially in time. This temporal decay is an explicit manifestation of the fact that, in the radiative range, true normal modes do not occur. The internal fields associated with the lattice motion couple with external radiative fields which extract energy from the mode, thus giving it a finite lifetime. It has been demonstrated[5] that a knowledge of the virtual modes leads to a detailed understanding of those optical properties of the slab associated with the lattice.

We are now going to apply the methods used to determine the collective excitations for the ionic crystal to determine the long-wavelength[6] collective excitations for the electrons in a metallic slab. The excitations we are concerned with involve the coupling between plasma-like electron motion and a photon field. One should not think of these excitations as a coupling between "ordinary" plasmons and photons since the plasmon is a longitudinal excitation. Rather, these are excitations associated with the modification of the photon dispersion curve by the metallic medium.[7] The "ordinary" plasmons, for which the frequency is the plasma frequency, exist for a slab, but they occur only for special wavelengths.[8]

The quantity of principal importance in determining the character of the long-wavelength excitations is the frequency-dependent dielectric constant. Thus in examining the collective excitations for a metallic slab, the appropriate expression for the dielectric constant is

$$\epsilon(\Omega,\gamma)=1-(\Omega^2+i\Omega\gamma)^{-1}, \qquad (1)$$

where $\Omega=\omega/\omega_P$ with ω_P the plasma frequency, and $\gamma=(\omega_P\tau)^{-1}$, τ being the (possibly frequency-dependent)

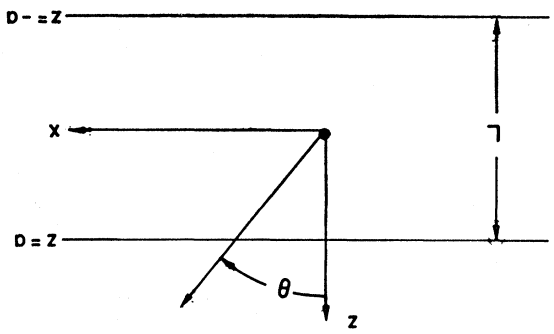

FIG. 1. A diagram giving the orientation of the slab, the thickness parameters, and the definition of θ.

* Work was performed in the Ames Laboratory of the U. S. Atomic Energy Commission. Contribution No. 1935.

[1] K. L. Kliewer and R. Fuchs, Phys. Rev. **144**, 495 (1966).

[2] K. L. Kliewer and R. Fuchs, Phys. Rev. **150**, 573 (1966).

[3] Of principal interest in the discussion of the ionic crystal were the modes with transverse character such that a direct interaction with photons was possible. There also exist, of course, longitudinal excitations for which $\omega=\omega_{LO}$, the ordinary long-wavelength longitudinal optical frequency. These modes are quantized in a slab, occurring as standing waves with the slab being an integral number of half-wavelengths thick. See Eqs. (2.54)–(2.61) of Ref. 1.

[4] ω is the angular frequency, k_x the wave vector in the x direction (see Fig. 1), and c the velocity of light. In the long-wavelength region, no loss of generality results from taking $k_y=0$.

[5] R. Fuchs, K. L. Kliewer, and W. J. Pardee, Phys. Rev. **150**, 589 (1966).

[6] The wavelength is to be long compared with the lattice parameter.

[7] In an infinite crystal, the photon dispersion curve is $\omega^2=k^2c^2$ if no interactions are included. Due to the presence of the minimum, the dispersion curve becomes $\omega^2=k^2c^2/\epsilon(\Omega,0)$ where the dispersion curve now describes an entity which is a mixture of electron motion and photons. $\epsilon(\Omega,0)$ is the undamped, frequency-dependent dielectric constant given in Eq. (1). The character of the excitations when the crystal is not infinitely thick is what concerns us here.

[8] The properties of these purely longitudinal excitations are described in Ref. 1 if one regards ω_L as the plasma frequency. See footnote 3 and the equations quoted therein. Nothing more will be said about these modes.

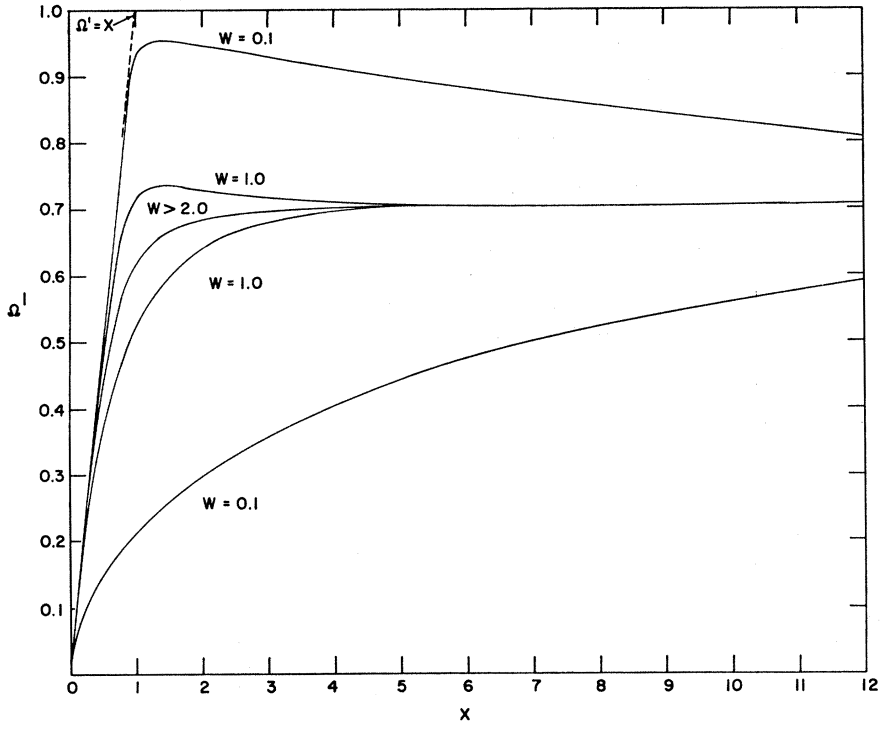

FIG. 2. Long-wavelength dispersion of the surface plasmons for various crystal thicknesses. The frequency is written as Ω' to emphasize the fact that these curves were calculated using $\epsilon(\Omega,0)$ with Ω real. Ω' always denotes the real part of the frequency. As $X \to 0$, all curves approach tangentially the line $\Omega'=X$, the free-space photon dispersion curve.

relaxation time. Considering that our interests are in excitations resulting from a coupling between electronic motion and electromagnetic waves, our adoption of (1) as the appropriate expression for ϵ involves the fact that the transverse and longitudinal dielectric constants are equal at large wavelengths.[9] In addition, the use of (1) indicates clearly that we are examining effects of essentially a free-electron character, rather than band effects.

A brief discussion of the long-wavelength dispersion of the surface plasmons is given in Sec. II. The virtual modes are presented and discussed in Sec. III. The optical properties of the slab are discussed in Sec. IV while Sec. V includes a general discussion of the philosophy of the calculation and of the applicability of the conclusions in analyzing various experimental results.

II. SURFACE PLASMONS

The only nonradiative excitations which occur for the metallic slab are the surface modes, since $\epsilon(\Omega,0)<1$ for all Ω.[10] The slab we are considering is shown in Fig. 1, free surfaces occurring at $z=\pm a$. Since a detailed solution of the complete set of Maxwell's equations has been given in Ref. 1, we will just quote the results here and then apply them to the case of a metal.

The dispersion curve for the high-frequency surface mode is given by[11]

$$\epsilon = -(\alpha/\alpha_0)\tanh\alpha a, \tag{2}$$

where

$$\alpha_0 = (k_x^2 - \omega^2/c^2)^{1/2} \tag{3}$$

and

$$\alpha = (k_x^2 - \epsilon\omega^2/c^2)^{1/2}. \tag{4}$$

The polarization[12] of the electron gas $\mathbf{P}(z)$ has components

$$\begin{aligned} P_x(z) &= C\sinh\alpha z, \\ P_z(z) &= -iC(k_x/\alpha)\cosh\alpha z, \end{aligned} \tag{5}$$

where C is a normalization constant.

For the low-frequency surface mode, the dispersion relation is

$$\epsilon = -(\alpha/\alpha_0)\coth\alpha a. \tag{6}$$

The associated polarization components are

$$\begin{aligned} P_x(z) &= C\cosh\alpha z, \\ P_z(z) &= -iC(k_x/\alpha)\sinh\alpha z. \end{aligned} \tag{7}$$

Since the solutions of Eqs. (2) and (6) of interest here occur for α real, ϵ is negative and, for large α, the

[9] W. Kohn, in *Optical Properties and Electronic Structure of Metals and Alloys*, edited by F. Abeles (North-Holland Publishing Company, Amsterdam, 1966), p. 1.

[10] This is evident from Fig. 3 of Ref. 1, which is modified in the following ways for a metal: (1) The horizontal line labeled $\epsilon=-\infty$ moves to $\omega/\omega_T=0$, causing the low-frequency regions R_1, L_1, and N_1 to disappear; (2) the frequency $\omega/\omega_T=2.2$ at which $\epsilon=0$ is now $\omega/\omega_T=1.0$; (3) the region L_1' disappears because the lines $\alpha=0$ and $\alpha_0=0$ [see Eqs. (3) and (4) below] no longer intersect. We are left with only the nonradiative regions N (where no modes exist) and L_2 (in which the surface modes exist), and the radiative regions R_1' and R_2.

[11] In Secs. II and III ϵ means $\epsilon(\Omega,0)$.

[12] The factor $e^{ik_x x}e^{-i\omega t}$ is to be understood in all polarization expressions.

polarization and the fields are localized at the surfaces. Hence these modes are denoted surface modes. The electromagnetic fields outside the slab go as $e^{-\alpha_0|z|}$.

The dispersion curves for these modes are given in Fig. 2 in terms of the dimensionless variables[13] $\Omega'=\omega/\omega_P$, $X=k_xc/\omega_P$. W is defined to be ω_PL/c where L is the thickness of the slab. $W=1.0$ corresponds to a thickness $L=4.0\times10^{-6}$ cm for a typical plasma energy, $E_P=5.0$ eV or $\omega_P=7.6\times10^{15}$ sec^{-1}. For a thin crystal ($W\lesssim1.0$), the interference of the fields at the two surfaces is different for solutions of opposite parity, resulting in different frequencies for the two types of surface modes. For a thick crystal the solutions become degenerate. If $X\gg1$, all frequencies approach the asymptotic limit $\Omega'=1/\sqrt{2}$, for which $\epsilon=-1$. This is the limit in which the surface plasmons occur at a frequency $\omega_P/\sqrt{2}$ and are identical to the longitudinal surface plasmons ($\nabla\times\mathbf{P}=0$) found when retardation is neglected. Note that the surface plasmons have electric field components in the x and z directions (Fig. 1) corresponding to P-polarized excitations. There exist no nonradiative surface excitations possessing S character.

The dispersion relations (2) and (6) have been derived previously from an alternative point of view.[14]

III. VIRTUAL MODES

The condition that characterizes the virtual modes[15] is that they correspond to energy transport out of the slab. Using this condition, together with a general solution of Maxwell's equations, the defining equations for the virtual modes can be obtained. For P polarizations the tangent equation is

$$-i\epsilon\beta_0/\beta=\tan\beta a, \tag{8}$$

where

$$\beta_0=(\omega^2/c^2-k_x^2)^{1/2} \tag{9}$$

and

$$\beta=(\epsilon\omega^2/c^2-k_x^2)^{1/2}. \tag{10}$$

The tangent equation yields virtual modes with the polarization components

$$\begin{aligned} P_x(z)&=C\sin\beta z,\\ P_z(z)&=(ik_xC/\beta)\cos\beta z. \end{aligned} \tag{11}$$

The cotangent equation for P polarization is

$$i\epsilon\beta_0/\beta=\cot\beta a \tag{12}$$

with the associated polarization components being

$$\begin{aligned} P_x(z)&=C\cos\beta z,\\ P_z(z)&=-(ik_xC/\beta)\sin\beta z. \end{aligned} \tag{13}$$

In the case of S polarization, the tangent equation is

$$-i\beta_0/\beta=\tan\beta a \tag{14}$$

with the polarization given by

$$P_y(z)\propto\cos\beta z, \tag{15}$$

whereas the cotangent equation is

$$i\beta_0/\beta=\cot\beta a, \tag{16}$$

for which the electronic polarization is

$$P_y(z)\propto\sin\beta z. \tag{17}$$

The dependent variable in the virtual mode equations is the complex frequency which we write as

$$\Omega=\Omega'+i\Omega''=\omega/\omega_P,$$

where Ω' gives the frequency of the mode and Ω'' is a measure of the frequency spread. Ω'' must be negative because of the requirement of temporal decay. The choice of the independent variable depends upon the particular physical situation of interest. In order for the angle θ (see Fig. 1) to be well defined for the virtual modes, k_x must be complex. In addition, k_x must have the same phase in the complex plane as ω, i.e., since $X=k_xc/\omega_P=X'+iX''$, we must have $X''/X'=\Omega''/\Omega'$. In this case $X=\Omega\sin\theta$ and θ can be considered the independent variable. The resultant modes, which we call the constant-angle virtual modes, are the only ones which will be discussed below since they are the modes which are directly related to optical studies.[16]

We now consider the two polarization types separately.

P Polarization

An idea as to the type of solution to be expected from Eqs. (8) and (12) can be obtained by examining the quantity ξ,

$$\xi=\epsilon\beta_0/\beta, \tag{18}$$

which appears on the left-hand side of these equations. Now ϵ, β, and β_0 will be complex quantities since Ω is complex, but it is illuminating to examine ξ considering all quantities to be essentially real. For small θ, $\xi\simeq\sqrt{\epsilon}$. Since ϵ is between zero and one for $\Omega\gtrsim1$, we would expect, for small θ, the tangent equation to have solutions for $\beta a\simeq n\pi$ and the cotangent equation to have solutions for $\beta a\simeq(n+\frac{1}{2})\pi$ with n an integer. This conclusion should be particularly valid for modes with $\Omega\sim1$, where $\epsilon\sim0$.

When $\theta\neq0$, we have

$$\xi=(1-\Omega^{-2})/(1-(\Omega\cos\theta)^{-2})^{1/2}. \tag{19}$$

The essential reality of βa means that in the limit $\theta\to90°$ Ω must diverge in such a fashion that $\Omega\cos\theta\gtrsim1$ with the result that $\xi>1$. Thus, for large angles, the

[13] The dimensionless frequency is written as Ω' here to emphasize the fact that ω is real now in contrast to the situation below.

[14] A figure is given on p. 103 of H. Raether, *Springer Tracts in Modern Physics* (Springer-Verlag, Berlin, 1965), Vol. 38, based upon the work of R. H. Ritchie and H. B. Eldridge, Phys. Rev. **126**, 1935 (1962).

[15] For details concerning this section, see Ref. 2.

[16] An alternative type of solution with k_x real is discussed in Ref. 2.

solutions of the tangent equation should occur for $\beta a \simeq (n+\frac{1}{2})\pi$, whereas the cotangent equation should have solutions for $\beta a \simeq n\pi$. This approximation should be best for the lowest frequency modes having $\Omega \cos \simeq 1$, since for these modes $\xi \gg 1$.

We conclude, therefore, that in following a particular solution of the tangent equation from $\theta=0$ to $\theta=90°$, βa should go from approximately an integral multiple of π to approximately an odd-integer multiple of $\frac{1}{2}\pi$ and vice versa for a cotangent mode. The transition in βa should occur for $\xi \sim 1$ or near the Brewster's angle ($\xi=1$ corresponds to $\tan\theta=\sqrt{\epsilon}$). In addition, modes of a given symmetry should alternate in frequency with modes of the opposite symmetry.

These arguments should be considered only as indicative of trends since the fact that the variables are complex complicates matters considerably. In particular the Brewster's-angle condition cannot rigorously occur when Ω is complex.

Consider $W=10.0$ (which is, on the scale of most of the effects we are concerned with, a thick crystal). The real and imaginary parts of the frequencies of the virtual modes are given in Fig. 3 as a function of the angle θ. Our comments above concerning the values of βa for the various modes are in accord with the detailed calculations. The $0T_1$ mode, a solution of the tangent equation [Eq. (8)], has both the real and imaginary parts of βa equal to zero at $\theta=0$ with Ω' equal to 1, the plasma frequency, and $\Omega''=0$. With increasing angle, $\mathrm{Re}(\beta a)$ for the $0T_1$ mode increases monotonically to $0.961(\frac{1}{2}\pi)$ as $\theta \to 90°$, whereas $\mathrm{Im}(\beta a)$ reaches a minimum of -0.696 at $\theta=31°$ and then increases to -0.299 as $\theta \to 90°$. This mode is unique in that the real part of the frequency is always below that corresponding to the Brewster's-angle frequency (calculated considering all quantities real), as indicated in Fig. 3.

The $1C_1$ mode, a solution of the cotangent equation [Eq. (12)], has $\mathrm{Re}(\beta a)=0.961(\frac{1}{2}\pi)$ at $\theta=0$, where $\mathrm{Im}(\beta a)=-0.299$. As $\theta \to 90°$, βa becomes $0.968\pi - i0.579$. Minima occur for Ω'' at $\theta=43°$ and for $\mathrm{Im}(\beta a)$ at $\theta=38°$, both relatively near the point where Ω' crosses the Brewster's-angle curve.

As is perhaps clear by now, the mode index is a measure of the $\theta=0$ value of $\mathrm{Re}(\beta a)$; that is, a mode labeled mC (mT) is a solution of the cotangent (tangent) equation with $\mathrm{Re}(\beta a) \simeq \frac{1}{2}m\pi$ for $\theta=0$. In particular this is true for the modes without a subscript in the label. In some cases, the $0T$ and $1C$ modes, which have the subscript 1, 2, or 3, are most peculiar and the index often ceases to have any real significance, becoming essentially a label. However, for any mode occurring at $\theta=0$, the above rule is roughly obeyed.

Several times above comments were made about the association of minima in $\mathrm{Im}(\beta a)$ and Ω'' with the angle for which Ω' crosses the Brewster's angle. The region near the Brewster's angle is characterized by ξ [Eq. (18)] being of the order of 1, which means that the real and imaginary parts of βa are roughly comparable and

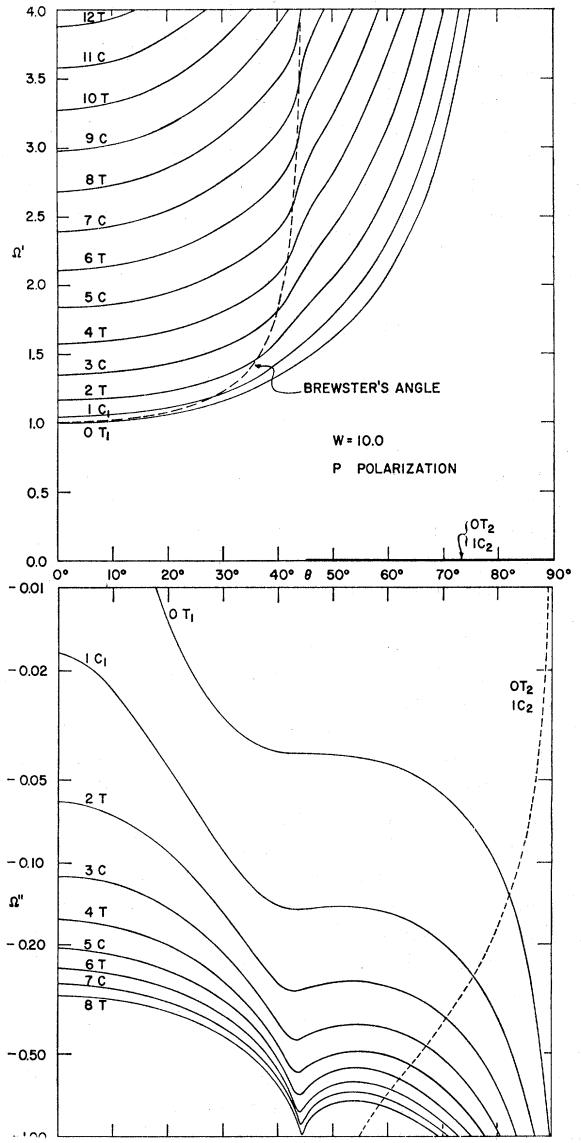

FIG. 3. The frequencies of the P-polarized virtual modes for $W=10.0$. The Brewster's-angle curve was calculated from the expression $\tan\theta=\sqrt{\epsilon}$ with $\epsilon=1-(\Omega')^{-2}$.

the ratio

$$\Gamma = |\Omega''|/\Omega' \tag{20}$$

is maximized. The physical reason for such behavior is as follows. The virtual modes represent an attempt by the crystal to establish, via multiple reflection, a standing wave pattern for the fields within. This is indicated by the values of $\mathrm{Re}(\beta a)$ for $\theta=0$ and 90°. In the vicinity of the Brewster's angle, the "transparency" of the crystal precludes effective multiple scattering, resulting in a deterioration of the field pattern. Thus the coupling of the internal fields with the external radiative fields is enhanced and the mode lifetime decreases. This corresponds to an increase in Γ and $|\mathrm{Im}(\beta a)|$ and is also

reflected in a relatively rapid change in $\mathrm{Re}(\beta a)$ and, hence, Ω'. As $\theta \to 90°$, $|\Omega''|$ increases without bound, as does Ω'; but Γ is significantly less than it is near the Brewster's angle, indicating further that the definition of the modes is poorest near the Brewster's angle.

The largest changes in Ω'' and Ω' and, from the arguments of the previous paragraph, those most closely associated with the Brewster's angle, occur for high-frequency modes in thick crystals ($W \gg 1$) and for all modes in thin crystals ($W \ll 1$). The reason for this is clear. In passing through the Brewster's angle $\mathrm{Re}(\beta a)$ must increase by approximately $\frac{1}{2}\pi$. Since βa is given by

$$\beta a = \tfrac{1}{2}(\epsilon - \sin^2\theta)^{1/2} W\Omega,$$

an increase in βa can occur when Ω increases because of the proportionality of βa to Ω and also because of the resultant increase in ϵ. When $\epsilon \sim 0$ ($\Omega \sim 1$), clearly a smaller change in Ω is necessary to produce the same change in βa than when Ω is large, because of the form of ϵ. It is also clear that when W is small the change in Ω necessary to change βa by a given amount is larger than when W is large.

We can illustrate some of the above points by comparing the values of Γ for various modes when $W = 10.0$ The $0T_1$ mode has Γ equal to 0 at $\theta = 0$, a maximum of 0.0300 for $\theta = 38°$, and 0.0166 as $\theta \to 90°$. For the $1C_1$ mode, Γ is 0.0166 at $\theta = 0$, 0.0978 at the minimum in Ω'', and 0.0518 as $\theta \to 90°$. Contrast this with the $9C$ mode for which Γ is 0.112 at $\theta = 0$, 0.241 at the Ω'' minimum ($\theta = 44°$), and 0.108 as $\theta \to 90°$. From these values and the curves of Fig. 3 it is clear that the definition of the modes decreases with increasing index, and that the peaks in $|\Omega''|$ and the rapid changes in Ω' are closely associated with the Brewster's angle for large mode indices.

One additional interesting feature is indicated in the numbers of the previous paragraph. We note that Γ for a cotangent (tangent) mode at $\theta = 90°$ is equal to Γ for the next higher tangent (cotangent) mode at $\theta = 0$. To demonstrate that this is a rigorous conclusion we compare the tangent equation for $\theta = 0$,

$$\tan\left\{\frac{W\Omega}{2}(1-\Omega^{-2})^{1/2}\right\} = -i(1-\Omega^{-2})^{1/2},$$

with the cotangent equation for $\theta \simeq 90°$,

$$\tan\left\{\frac{W}{2}(\Omega\cos\theta)(1-(\Omega\cos\theta)^{-2})^{1/2}\right\} \simeq -i(1-(\Omega\cos\theta)^{-2})^{1/2}.$$

These equations are of the same form, Ω in the $\theta = 0$ equation being replaced by $\Omega\cos\theta$ in the $\theta \simeq 90°$ equation. Considering Ω as essentially real, we have shown that the values of βa for these two cases should be comparable. It is now clear that they should be identical, and thus $(\Omega\cos\theta)_{\text{mode } m \text{ at } 90°} \equiv (\Omega)_{\text{mode } (m+1) \text{ at } 0°}$. The equality of Γ for the two cases follows immediately.

It was pointed out above that the most well-defined mode is the $0T_1$ mode. In addition it is an extremely important entity, being the mode from which Ferrell predicted "plasma radiation" should be emitted[17] and also the mode McAlister and Stern utilized in making the first optical determination of the plasma frequency.[18] We now will examine analytically some of the properties of this mode.

Since the $0T_1$ mode occurs for $\beta a \sim 0$ for low angles, we write $\tan\beta a = \beta a$, so that Eq. (8) becomes

$$(W\Omega/2)(\epsilon - \sin^2\theta) = -i\epsilon\cos\theta. \tag{21}$$

For $\theta = 0$, it is immediately apparent that the solution is $\epsilon = 0$ or $\Omega' = 1.0$ and $\Omega'' = 0$. Thus this mode always occurs at the plasma frequency for $\theta = 0$ independent of the thickness of the crystal.

Suppose now that $\theta \neq 0$. Then, writing the complex frequency and dielectric constant in polar form as

$$\begin{aligned} \Omega &= \Omega_p e^{i\phi}, \\ \epsilon = \epsilon' + i\epsilon'' &= \epsilon_p e^{i\eta}, \end{aligned} \tag{22}$$

we get from (21) the pair of equations

$$\tfrac{1}{2}W\Omega_p\{\epsilon_p\cos\eta - \sin^2\theta\} = \epsilon_p\cos\theta\sin(\eta-\phi), \tag{23}$$

$$\tfrac{1}{2}W\Omega_p\sin\eta = -\cos\theta\cos(\eta-\phi). \tag{24}$$

Since the $0T_1$ mode occurs for $\Omega' \sim 1$, $\Omega'' \sim 0$, let us consider a thick crystal for which $W\Omega_p/2 \gg 1$ and assume $\phi \sim 0$. From (24),

$$\tan\eta = -2\cos\theta/W\Omega_p,$$

so $\eta \sim 0$. Using (23) we see then that $\epsilon_p\cos\eta \simeq \sin^2\theta$ or $\epsilon_p \simeq \sin^2\theta$. Since $|\eta|$ is small, $\epsilon' \simeq \epsilon_p$ and

$$\epsilon'' \simeq -2\sin^2\theta\cos\theta/W\Omega_p.$$

Thus,

$$\Omega' \simeq (\cos\theta)^{-1} \tag{25}$$

and, since

$$\epsilon'' \simeq 2\Omega''/(\Omega')^3,$$

Ω'' is given by

$$\Omega'' \simeq -\sin^2\theta/(W\cos\theta). \tag{26}$$

Note that $\Omega'' \propto W^{-1}$.

Consider now $W\Omega_p/2 \ll 1$. Then $\eta \simeq -\pi/2$, $\epsilon_p \simeq (W\Omega_p/2)(\sin^2\theta/\cos\theta)$, and $\epsilon'' \simeq -\epsilon_p$. Thus,

$$\Omega'' \simeq -W\sin^2\theta/4\cos\theta \tag{27}$$

and

$$\Omega' \simeq 1 + \tfrac{1}{8}W^2\tan^2\theta. \tag{28}$$

Note that $\Omega'' \propto W$.

These conclusions concerning the $0T_1$ mode are valid for βa small or for angles less than about 45°. For a given angle in this range, Ω'' will be a maximum for $W \sim 2$, as is indicated by Eqs. (26) and (27). Equations (25) and (26) accurately represent the frequencies of the $0T_1$ mode in Fig. 3 for $\theta \lesssim 45°$. The case of a thin crystal will be illustrated below. It should be noted

[17] R. A. Ferrell, Phys. Rev. **111**, 1214 (1958).
[18] A. J. McAlister and E. A. Stern, Phys. Rev. **132**, 1599 (1963).

that βa being small for the $0T_1$ mode at low angles means that the polarization is essentially uniform in the z direction and zero in the x direction.

There are unique modes appearing in Fig. 3 which have not yet been mentioned. These are the $0T_2$ and $1C_2$ modes, which exist only for $\theta \geq 45°$ and have $\Omega' = 0$. As will be shown below, these modes play an important role in determining the low-frequency optical behavior of a slab, and thus we will examine their properties in detail.

Consider the tangent equation with $\Omega' = 0$,

$$\tanh\left[\frac{W\Omega''}{2}\left(\cos^2\theta + \frac{1}{(\Omega'')^2}\right)^{1/2}\right] = -\frac{\cos\theta\{1+1/(\Omega'')^2\}}{(\cos^2\theta+1/(\Omega'')^2)^{1/2}}. \quad (29)$$

As $\theta \to 90°$, Eq. (29) becomes

$$\tanh(\tfrac{1}{2}W) \simeq -\cos\theta/\Omega'',$$

so that

$$\Omega'' \simeq -\cos\theta/\tanh(\tfrac{1}{2}W). \quad (30)$$

Similarly, the cotangent equation, with $\Omega' = 0$, becomes

$$\coth\left[\frac{W\Omega''}{2}\left(\cos^2\theta + \frac{1}{(\Omega'')^2}\right)^{1/2}\right] = -\frac{\cos\theta\{1+1/(\Omega'')^2\}}{(\cos^2\theta+1/(\Omega'')^2)^{1/2}}, \quad (31)$$

which has a solution, in the limit $\theta \to 90°$,

$$\Omega'' \simeq -\cos\theta/\coth(\tfrac{1}{2}W). \quad (32)$$

Equations (30) and (32) are valid for all W as long as $(\Omega'')^2 \ll 1$.

With decreasing angle, $|\Omega''|$ increases rapidly as indicated in Fig. 3. When $W|\Omega''|/2 \gg 1$, the solution of Eqs. (29) and (31) is

$$\Omega'' = -\cos\theta/(1-2\cos^2\theta)^{1/2}, \quad (33)$$

from which it is clear that a solution exists only for $\theta \geq 45°$ and that $\Omega'' \to -\infty$ as $\theta \to 45°$. The equality of Eqs. (30) and (32) for $W \gg 1$, together with Eq. (33), demonstrate the fact that the $1C_2$ and $0T_2$ modes are degenerate in frequency for a thick crystal. In addition, it should be noted, and this is an extremely important point, that the $0T_2$ and $1C_2$ modes as given in Fig. 3 for $W = 10.0$ are thick-crystal solutions and, as such, are unchanged for larger W, even $W \to \infty$. This is not true of the other modes of Fig. 3.

The polarization of the electron gas associated with the $0T_2$ mode is

$$P_x(z) \propto \sinh\left[\frac{W\Omega''}{2}\left(\cos^2\theta + \frac{1}{(\Omega'')^2}\right)^{1/2}\frac{z}{a}\right],$$
$$P_z(z) \propto \sin\theta\cosh\left[\frac{W\Omega''}{2}\left(\cos^2\theta + \frac{1}{(\Omega'')^2}\right)^{1/2}\frac{z}{a}\right], \quad (34)$$

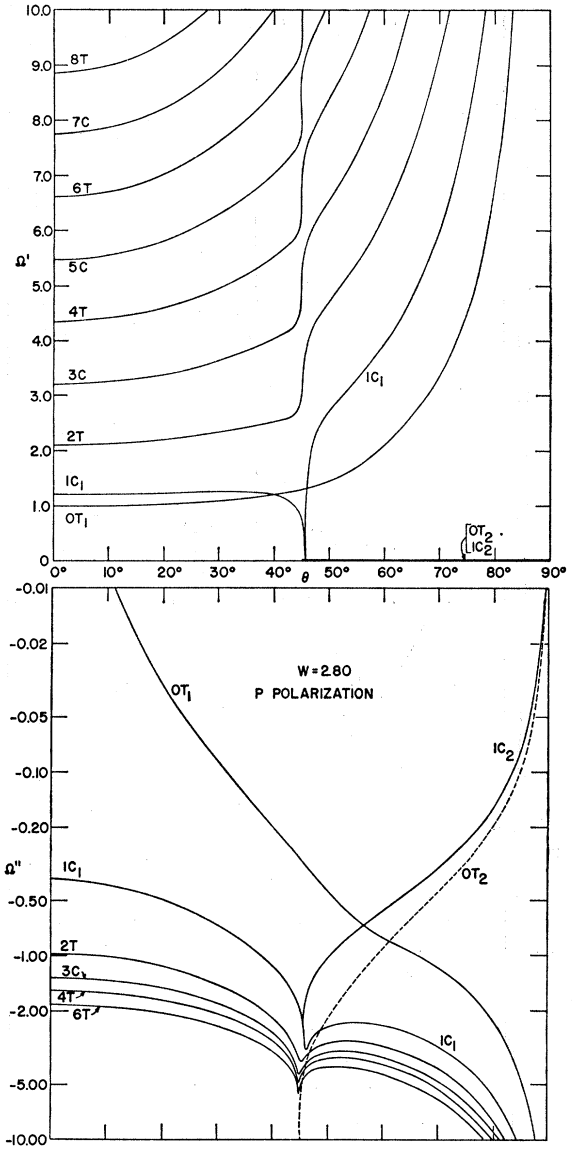

FIG. 4. The frequencies of the P-polarized virtual modes for $W = 2.80$.

identifying this mode clearly as a surface mode. Near 90°, where Ω'' is small,

$$P_x(z) \propto -\sinh(Wz/2a),$$
$$P_z(z) \propto \sin\theta\cosh(Wz/2a). \quad (35)$$

Similarly, the polarization components near 90° for the $1C_2$ mode, also a surface mode, are

$$P_x(z) \propto \cosh(Wz/2a),$$
$$P_z(z) \propto -\sin\theta\sinh(Wz/2a). \quad (36)$$

In Fig. 4, the frequencies of the virtual modes are given for a crystal with $W = 2.80$. Ω' for the $0T_1$ mode is essentially the same as it was for $W = 10.0$ [see Eq. (25)], but $|\Omega''|$ has increased in accord with the

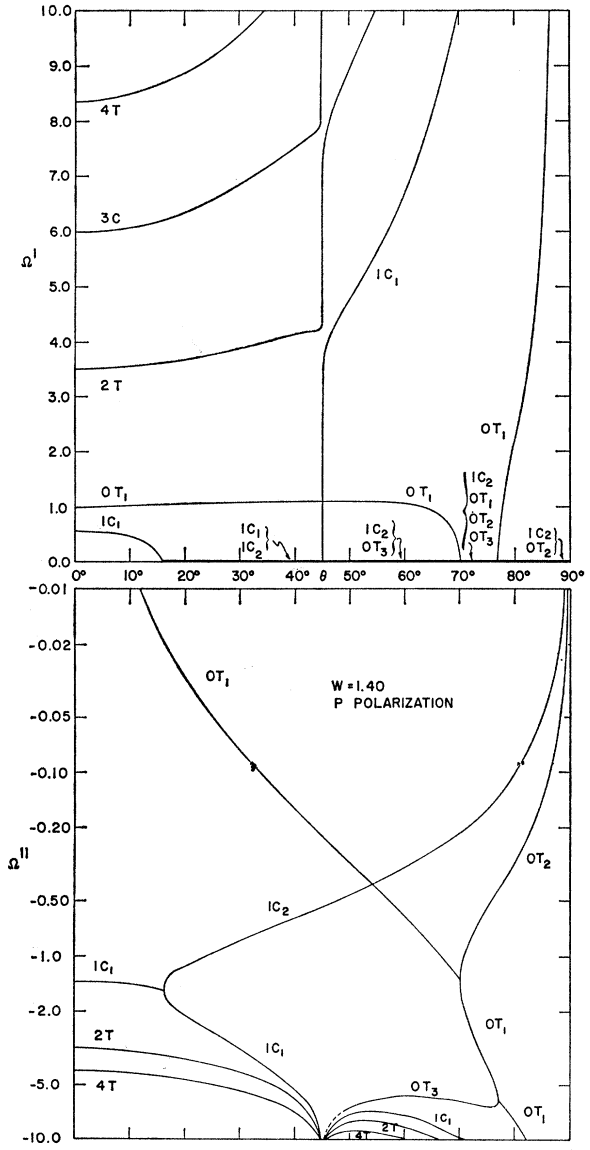

FIG. 5. The frequencies of the P-polarized virtual modes for $W=1.40$. Ω'' for the $0T_3$ mode approaches $-\infty$ as $\theta \rightarrow 45°$.

W^{-1} dependence given by Eq. (26). The reduction in thickness from $W=10.0$ results in the modes being more widely spaced in Ω', as expected from the form of β, and the transitions in Ω' and $\mathrm{Re}(\beta a)$ are somewhat more pronounced as anticipated from the arguments above. The transitions in Ω' are rather closely associated with the Brewster's angle as are the sharp dips in Ω''. At $\theta=0$, $\mathrm{Re}(\beta a)$ is $0.718(\frac{1}{2}\pi)$ for the $1C_1$ mode, 0.850π for the $2T$ mode, and $2.74(\frac{1}{2}\pi)$ for the $3C$ mode, indicating that the mode index is a meaningful quantity.

Important new features in Fig. 4 are the onset of critical behavior in the $1C_1$ mode and the separation of the $0T$ and $1C_2$ modes. For $\theta \simeq 46°$, Ω' for the $1C_1$ mode drops abruptly to zero and then rapidly increases. Near 90° the separation of the $0T_2$ and $1C_2$ modes follows from the fact that $\frac{1}{2}W$ is now of the order of 1, $\tanh(W/2) < \coth(W/2)$, and thus $|\Omega''|$ for the $0T_2$ mode is greater than for the $1C_2$ mode [see Eqs. (30) and (32)]. In addition, the cotangent equation no longer has a solution which diverges for $\theta \rightarrow 45°$, the $1C_2$ mode joining the $1C_1$ mode in the critical region. The $0T_2$ mode has Ω'' given by Eq. (33) for $W|\Omega''|\cos\theta \gg 1$.

That there should be a critical thickness below which the $1C_2$ mode ceases to diverge as $\theta \rightarrow 45°$ is clear. We saw above that Ω'' diverges for $W=10.0$. For small W, Eq. (32) indicates that $|\Omega''| \ll 1$ for all θ. Then Eq. (32)

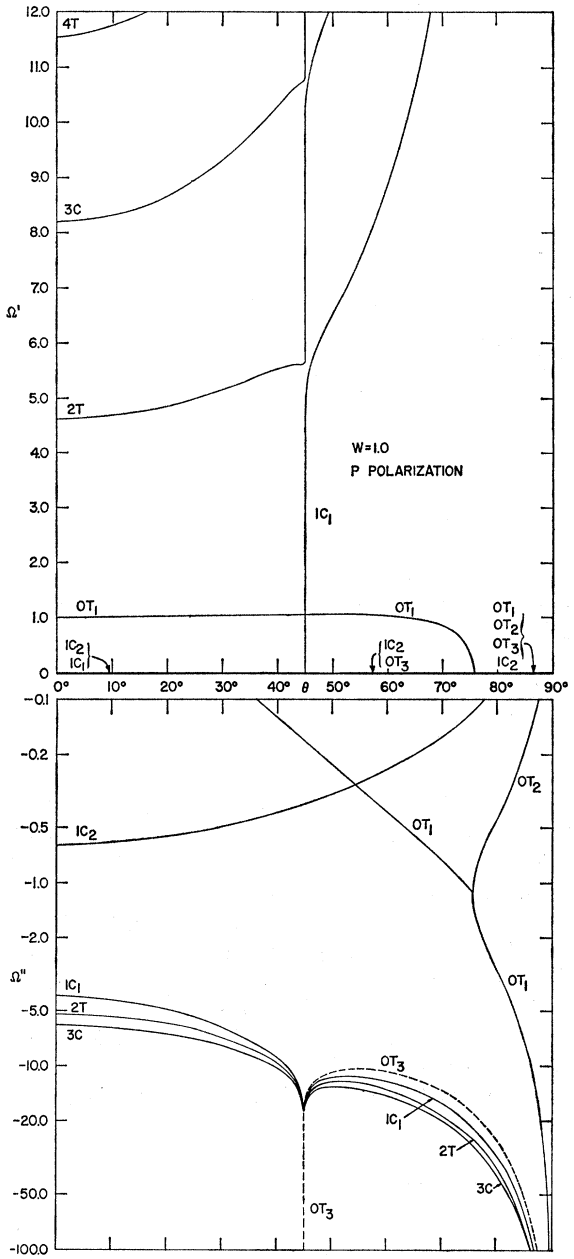

FIG. 6. The frequencies of the P-polarized virtual modes for $W=1.0$.

is a valid expression for Ω'' for all θ and there is no divergent behavior. The critical thickness is $W\sim 3$.

Decreasing W to 1.40 results in further complications as indicated in Fig. 5. The modes with indices $\gtrsim 2$ behave in rather standard fashion, but the same cannot be said for the $0T$ or $1C$ modes. The $0T_1$ mode has the usual frequencies for $\theta=0$. However, for $\theta\simeq 70°$ Ω' goes to zero at the point where the $0T_1$ and $0T_2$ modes join. Ω' increases abruptly for the $0T_1$ mode near $\theta=77°$, where the $0T_1$ and $0T_3$ modes merge. $0T_3$ is the divergent mode as $\theta\to 45°$ while $0T_2$ has $\Omega''\to 0$ as $\theta\to 90°$, in accord with Eq. (30).

The $1C_1$ mode at $\theta=0$ has $\mathrm{Re}(\beta a)=0.209(\pi/2)$. This, together with the fact that $\Gamma=2.41$ at $\theta=0$, indicates this mode is now very ill-defined. Ω' goes to zero for $\theta\simeq 16°$, where the $1C_1$ and $1C_2$ modes connect. At $\theta\simeq 45°$, Ω' for the $1C_1$ mode rises abruptly,[19] whereas the $1C_2$ mode continues with Ω' equal to zero. Ω'' for the $1C_2$ mode is given by Eq. (32) for $\theta\gtrsim 45°$.

Figure 6 gives the virtual mode frequencies for $W=1.0$. Since this is a reasonably thin crystal, Ω' and Ω'' for the $0T_1$ mode are relatively well represented by Eqs. (28) and (27) for $\theta\lesssim 45°$. Note that Ω' for moderate angles remains near 1.0, being 1.05 for $\theta=45°$, and also that Ω' no longer diverges as $\theta\to 90°$. The $1C_1$ and $1C_2$ modes are once again distinct with Ω'' for the $1C_2$ mode now given by (32) for all θ. The $0T_2$ mode is well described by Eq. (30) and there are now two $0T$ modes with $\Omega''\to-\infty$ as $\theta\to 90°$: $0T_1$ and $0T_3$.[20] The $0T_3$ mode remains the divergent mode as $\theta\to 45°$.

Considering, finally, a thin crystal, the mode frequencies for $W=0.20$ are given in Fig. 7. Ω' for the $0T_1$ mode, given by Eq. (28), is essentially 1.0 if $\theta\lesssim 80°$. Ω'' and Ω' are accurately given by Eqs. (27) and (28) if $\theta\lesssim 45°$. Expressions for Ω'' are given by Eq. (32) for the $1C_2$ mode for all values of θ and by Eq. (30) for the now very compressed $0T_2$ mode. Ω'' diverges as $\theta\to 90°$ for the $0T_1$ and $0T_3$ modes and as $\theta\to 45°$ for the $0T_3$ mode.

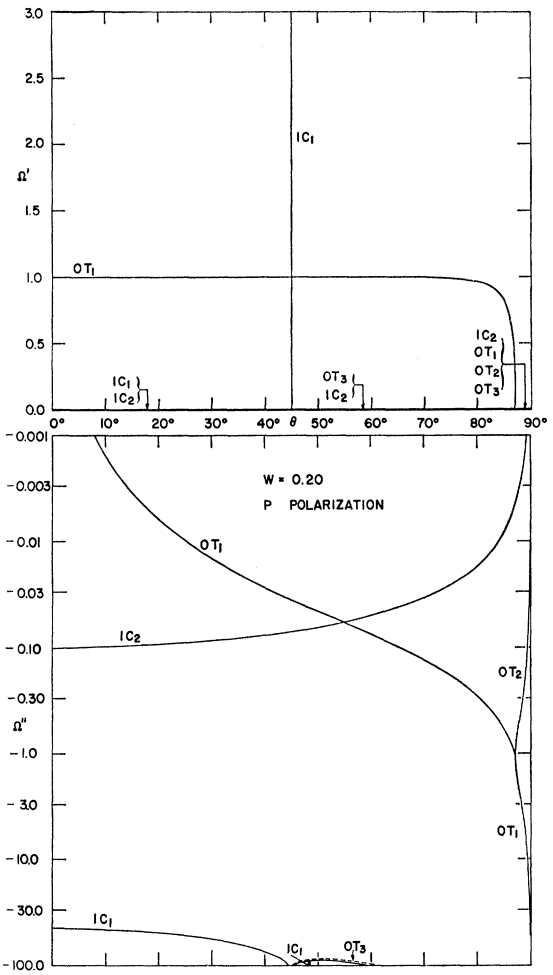

FIG. 7. The frequencies of the P-polarized virtual modes for $W=0.20$. Ω'' for the $0T_3$ mode diverges for $\theta\to 45°$ and for $\theta\to 90°$.

S Polarization

For the case of S polarization, the virtual mode equations are (14) and (16). There is no feature for S polarization analogous to the Brewster's angle for P polarization, as is indicated mathematically by the fact that ϵ does not appear on the left side of these equations, as it does for P polarization. Thus we expect that βa will be roughly the same at $\theta=0$ as at 90°.[21]

There are, however, some distinct similarities in the two polarization types. The tangent equation for P polarization at $\theta=0$ is $\tan\beta a=-i\epsilon^{1/2}$, which is just the $\theta=0$ cotangent equation for S polarization. Thus, the $\theta=0$ tangent frequencies for P polarization are the $\theta=0$ cotangent frequencies for S polarization, and vice versa. For $\theta\to 90°$, the S and P tangent frequencies are identical as are the S and P cotangent frequencies. In order to retain the meaning of the mode index as the approximate value of $\mathrm{Re}(\beta a)$ for $\theta=0$, we must now associate even integers with the cotangent modes and odd integers with the tangent modes.

In Fig. 8, the frequencies of the virtual modes are given for $W=1.4$. Comparing Fig. 8 with Fig. 5, we see that for $\theta=0$, the mode of index m for S polarization

[19] This abrupt rise is directly associated with the Brewster's angle since, below the transition, $|\Omega''|$ is large, $\epsilon\simeq 1$, and $\theta_B=\tan^{-1}\sqrt{\epsilon}\simeq 45°$.

[20] Since we are concerned here with $0T$ modes having $\Omega'=0$, it is easy to show that the divergent values of Ω'' as $\theta\to 90°$ are solutions of

$$\Omega''\simeq-(W\cos\theta)^{-1}[1\pm(1-W^2)^{1/2}].$$

For $W\ll 1$, there are two solutions: $\Omega''=-2/W\cos\theta$, the $0T_3$ mode, and $\Omega''=-W/2\cos\theta$, the $0T_1$ mode. The above general expression for Ω'' suggests that there are solutions with divergent Ω'' and $\Omega'=0$ as $\theta\to 90°$ only for $W<1$. In fact there are still two such solutions for $W=1.0$ (Fig. 6) because βa is not sufficiently small that the expansion $\tan\beta a=\beta a$ is accurate.

[21] Actually, βa is a constant, independent of angle, for a given mode.

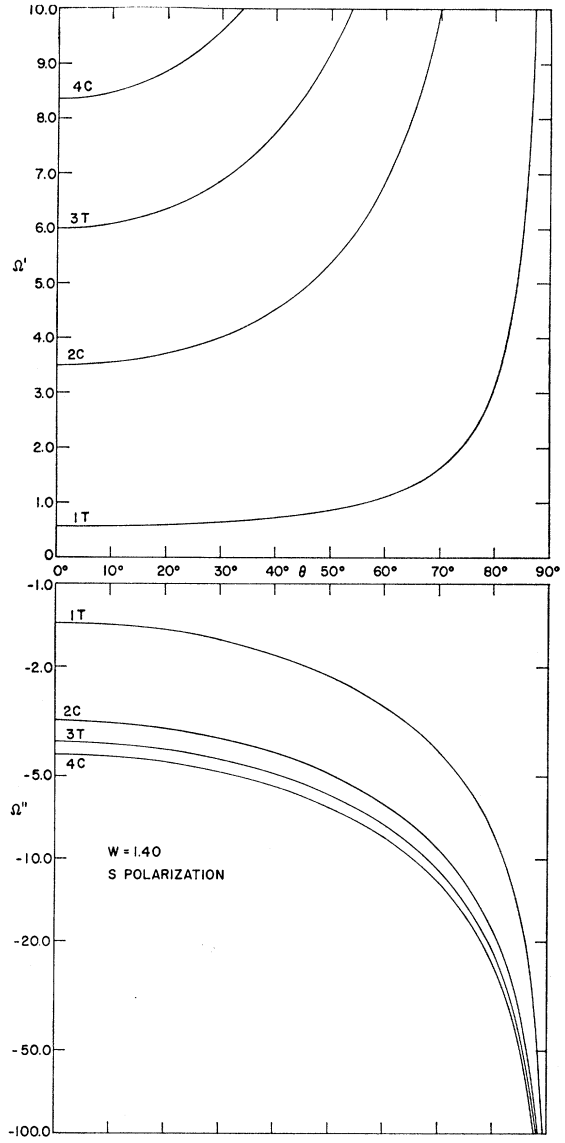

FIG. 8. The frequencies of the S-polarized virtual modes for $W=1.40$.

has the same frequencies as the mode of index m for P polarization, whereas for $\theta\rightarrow 90°$, the mode of index m for S polarization has the same frequencies as the mode of index $(m-1)$ for P polarization.

The modes for S polarization are seen to be considerably less exciting than for P polarization. In particular, there are no modes for S polarization analogous to the $0T_2$ mode and the $0T_1$ mode at small angles. The S-polarized mode $1T$ which corresponds to $1C_1$ for small θ becomes identical to the $0T_1$ mode at $\theta\rightarrow 90°$. For a thinner crystal ($W\leq 1$), the $\Omega'=0$ S-polarized modes corresponding to P-polarized $1C_1$ and $1C_2$ for small θ become identical to $0T_3$ and $0T_1$ when $\theta\rightarrow 90°$.

TABLE I. Virtual modes for P polarization. $W=10$.

Mode	θ	$\eta'+i\eta''$	$\rho'+i\rho''$	f'	$A_{\max}$
$0T_1$	0°	$1.0002-0i$	$1.0000-0.0100i$	1.00	0
	10°	$1.0150-0.0030i$	$1.0150-0.0130i$	1.00	0.36
	45°	$1.4583-0.0404i$	$1.4589-0.0501i$	0.96	0.31
	75°	$4.0282-0.0562i$	$4.0287-0.0803i$	0.93	0.16
$1C_1$	0°	$1.0433-0.0173i$	$1.0436-0.0266i$	0.93	0.50
	10°	$1.0584-0.0237i$	$1.0588-0.0330i$	0.93	0.41
	30°	$1.2143-0.0904i$	$1.2154-0.0998i$	0.94	0.17
	45°	$1.5943-0.1490i$	$1.5963-0.1573i$	0.83	0.10
	75°	$4.5000-0.2472i$	$4.5012-0.2547i$	0.75	0.08
$2T$	0°	$1.1664-0.0604i$	$1.1676-0.0679i$	0.75	0.26
	10°	$1.1834-0.0675i$	$1.1846-0.0750i$	0.75	0.18
	30°	$1.3434-0.1515i$	$1.3450-0.1591i$	0.76	0.09
	45°	$1.8222-0.2927i$	$1.8253-0.2990i$	0.63	0.04
	75°	$5.2152-0.4589i$	$5.2168-0.4644i$	0.56	0.02
$0T_2$	50°	$0-1.5426i$	$0-1.5526i$	1.00	0.01
and	60°	$0-0.7072i$	$0-0.7173i$	1.00	0.03
$1C_2$	75°	$0-0.2782i$	$0-0.2883i$	1.02	0.07
	85°	$0-0.0878i$	$0-0.0984i$	1.27	0.23

IV. OPTICAL PROPERTIES

The foregoing virtual modes were obtained with zero intrinsic damping for the electron gas. Absorption[22] of light by the metallic slab can occur only if the damping parameter in the dielectric constant $\epsilon(\Omega,\gamma)$ of Eq. (1) is different from zero. It has been shown, for constant γ, that each virtual mode is associated with a peak in the optical absorption.[5] If the frequency of a virtual mode has been determined for both $\gamma=0$ and $\gamma\neq 0$, the position, width, and height of the absorption peak can be calculated.

Suppose that P-polarized light of frequency Ω is incident on the slab. Then the absorption coefficient A can be written[5]

$$A=A_1+A_2, \tag{37}$$

where

$$A_1=\frac{L_1+L_1^*-2}{|L_1|^2}, \qquad A_2=\frac{L_2+L_2^*-2}{|L_2|^2}, \tag{38}$$

with

$$L_1=1-(i\beta/\beta_0\epsilon)\tan\beta a, \qquad L_2=1+(i\beta/\beta_0\epsilon)\cot\beta a. \tag{39}$$

When the frequency is real, A_1 and A_2 each represent the absorption due to the modes of a given parity. The angle of incidence measured from the z axis is θ, defined by $k_x c=\omega\sin\theta$ as in Sec. III. If the frequency is allowed to become complex, the equations $L_1=0$ and $L_2=0$ are the same as Eqs. (8) and (12) for the virtual modes.

[22] By the terms "absorption" A, "reflection" R, and "transmission" T in an optical experiment, we refer, respectively, to the fraction of the incident power absorbed, reflected, and transmitted by the entire slab. The terms "absorptance," "reflectance," and "transmittance" are more commonly used for these quantities.

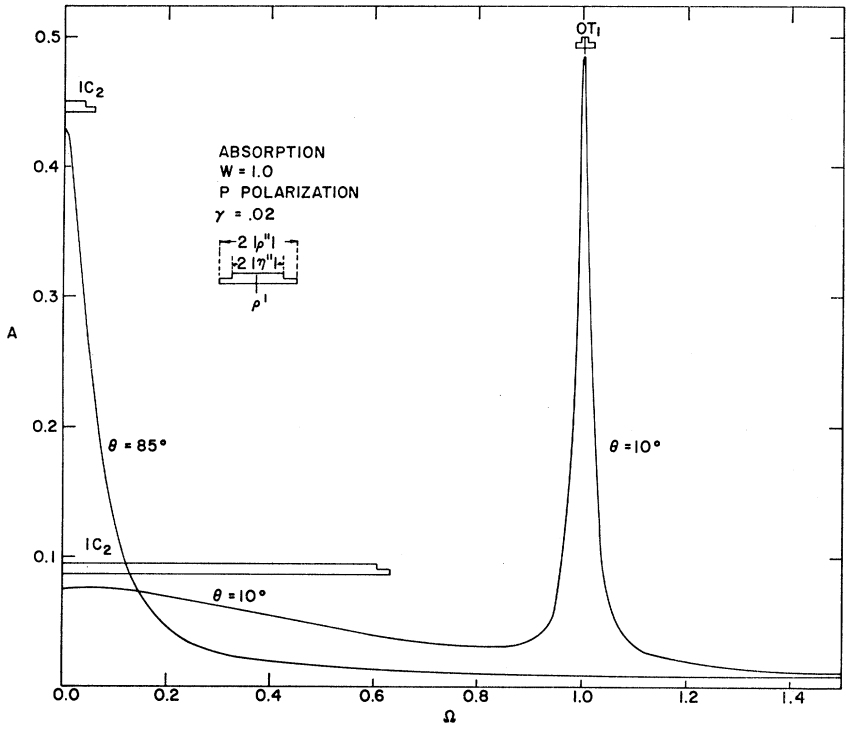

FIG. 9. Absorption as a function of frequency for P polarization and thickness $W=1.0$.

For S-polarized light, the factor ϵ in Eqs. (39) is missing.

The contribution to the absorption A_1 made by an individual virtual mode of type I (a tangent mode) is a Lorentzian peak given by

$$A_1=\frac{2\eta''\Delta\Omega''}{(\Omega-\rho')^2+(\rho'')^2}, \tag{40}$$

where Ω is the real frequency of the incident light, $\eta'+i\eta''$ is the frequency of the virtual mode when $\gamma=0$, $\rho'+i\rho''$ is the frequency when $\gamma\neq 0$, and $\Delta\Omega''$ $=\rho''-\eta''$ is the change in the imaginary part of the frequency when γ is included. η'' and ρ'' are negative quantities and, normally, so is $\Delta\Omega''$. An expression similar to (40) holds for A_2. Since the absorption peaks due to virtual modes of the same parity are not additive, Eq. (40) describes the absorption accurately only if modes of the same parity are far enough apart that the associated absorption peaks do not overlap significantly. This requirement is a consequence of the approximation used in deriving Eq. (40), namely, that in the neighborhood of a virtual mode, L_1 can be represented by an expression linear in Ω. This linear approximation breaks down if the virtual modes are close together or if the imaginary part of the frequency of a virtual mode is too large ($|\eta''|\gtrsim 1$).

We now show the effect on typical virtual modes when γ is changed from 0 to 0.02. Tables I, II, and III

TABLE II. Virtual modes for P polarization. $W=1.0$.

Mode	θ	$\eta'+i\eta''$	$\rho'+i\rho''$	f'	$A_{\max}$
$0T_1$	0°	$1.0000-0i$	$1.0000-0.0100i$	1.00	0
	10°	$1.0030-0.0062i$	$1.0029-0.0162i$	1.01	0.47
	30°	$1.0253-0.0627i$	$1.0249-0.0731i$	1.05	0.24
	45°	$1.0469-0.1689i$	$1.0456-0.1800i$	1.11	0.12
	75°	$0.3915-1.075i$	$0.3587-1.088i$	1.33	0.02
	80°	$0-2.964i$	$0-2.993i$	2.96	0.02
	85°	$0-6.872i$	$0-6.899i$	2.67	0.01
$0T_2$	80°	$0-0.4490i$	$0-0.4465i$	−0.25	−0.01
	85°	$0-0.1958i$	$0-0.1968i$	0.10	0.01
	89°	$0-0.0378i$	$0-0.0405i$	0.27	0.12
$0C_2$	0°	$0-0.6241i$	$0-0.6504i$	2.62	0.08
	10°	$0-0.6064i$	$0-0.6322i$	2.57	0.08
	30°	$0-0.4896i$	$0-0.5126i$	2.30	0.09
	45°	$0-0.3697i$	$0-0.3904i$	2.09	0.10
	75°	$0-0.1214i$	$0-0.1401i$	1.88	0.23
	85°	$0-0.0403i$	$0-0.0589i$	1.86	0.43

TABLE III. Virtual modes for P polarization. $W=0.2$.

Mode	θ	$\eta'+i\eta''$	$\rho'+i\rho''$	f'	$A_{\max}$
$0T_1$	0°	$1.0000-0i$	$1.0000-0.0100i$	1.00	0
	10°	$1.0000-0.0015i$	$1.0000-0.0115i$	1.00	0.23
	45°	$1.0017-0.0269i$	$1.0014-0.0369i$	1.00	0.40
	75°	$0.9882-0.1813i$	$0.9863-0.1914i$	1.01	0.10
$0T_2$	88°	$0-0.4085i$	$0-0.4047i$	−0.39	−0.02
	89°	$0-0.1808i$	$0-0.1802i$	−0.06	−0.07
$1C_2$	0°	$0-0.1007i$	$0-0.1208i$	2.01	0.28
	10°	$0-0.0991i$	$0-0.1192i$	2.01	0.28
	45°	$0-0.0708i$	$0-0.0909i$	2.00	0.34
	75°	$0-0.0258i$	$0-0.0458i$	2.00	0.49

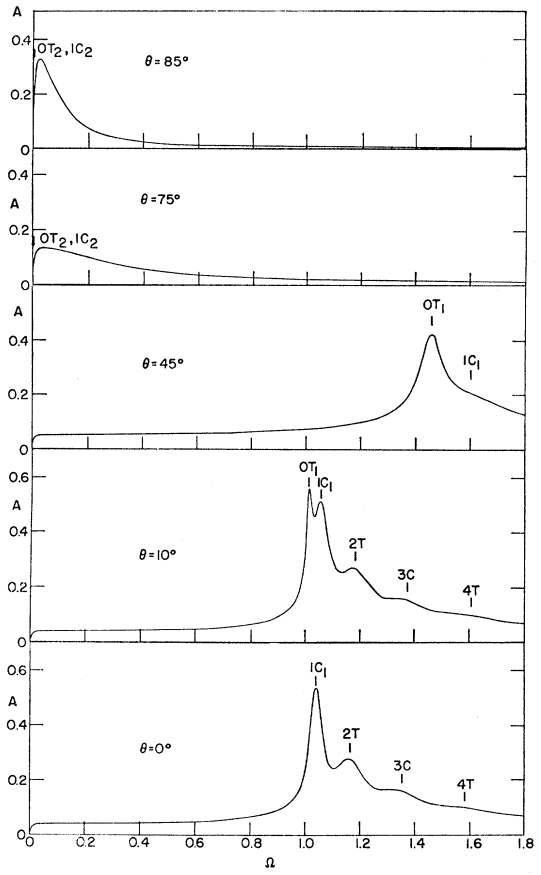

FIG. 10. Absorption as a function of frequency for P polarization and thickness $W=10.0$.

show the mode label, the angle θ, the frequency $\eta'+i\eta''$ when $\gamma=0$, the frequency $\rho'+i\rho''$ when $\gamma=0.02$, and a factor f' defined by $\Delta\Omega''=-(\frac{1}{2}\gamma)f'$ from which it can be seen immediately how the addition of γ changes the imaginary part of the frequency. Setting $\Omega=\rho'$ in Eq. (40) gives an expression for the peak absorption at the center of an absorption line,

$$A_{\max}=\gamma f'|\eta''|/(\rho'')^2. \tag{41}$$

The values of $A_{\max}$ in the last column thus show how large a contribution to the absorption each virtual mode makes. For the normal virtual modes the real part of the frequency changes very little, while the change in the imaginary part of the frequency is given by f' on the order of unity. It follows from Eq. (40) that the position of the absorption peak associated with such a virtual mode does not depend on γ, but that the width increases over the purely radiative width by about $\frac{1}{2}\gamma$. In a few cases $f'<0$; Eqs. (40) or (41) would then imply that the width of the absorption peak decreases with increasing γ and that the absorption itself is negative. This surprising formal result does not imply that the total absorption can become negative, which would be impossible. For those modes with $f'<0$ either (1), the imaginary part of the frequency is so large and negative ($\rho''\lesssim-1$) that Eq. (40) cannot be expected to hold, or (2), for those cases when Eq. (40) should apply (e.g., the $0T_2$ mode for $W=1.0$ and $W=0.2$), the negative absorption is more than canceled by the positive absorption due to other modes.

Figures 9 and 10 show the result of an exact calculation of the absorption as a function of frequency with $\gamma=0.02$, using Eqs. (37), (38), and (39). The two curves in Fig. (9) are for the angles of incidence $\theta=10°$ and $\theta=85°$ and a slab thickness $W=1.0$. Each absorption peak is labeled by the symbol for the associated virtual mode and by a double bar showing the frequency ρ' at which the peak should be centered, and by the widths $|2\eta''|$ when $\gamma=0$ and $|2\rho''|$ when $\gamma=0.02$. If $\theta=10°$ there is a broad peak at $\Omega=0$ due to the $1C_2$ mode and a narrow peak at $\Omega=1.003$ due to the $0T_1$ mode. When $\theta=85°$ the $1C_2$ peak at $\Omega=0$ has become higher and narrower. At this angle the $0T_1$ mode has evolved into two zero-frequency modes, $0T_1$ and $0T_2$. These modes contribute very little to the peak at $\Omega=0$, and therefore are not included in the figure as labels for this peak.

Figure 10 shows the absorption as a function of frequency for a slab thickness $W=10.0$ and a series of five angles. When $\theta=0°$, peaks due to the $1C_1$, $2T$, $3C$, and $4T$ modes are visible; there is no $0T_1$ peak at normal incidence. When $\theta=10°$, the $0T_1$ peak has appeared and the other peaks have moved to slightly higher frequencies. As θ continues to increase, these peaks move to still higher frequencies and are off the graph to the right when $\theta=75°$. The zero-frequency modes $0T_2$ and $1C_2$ come into existence when $\theta>45°$, and the associated peak at $\Omega=0$ becomes higher and narrower as θ increases to 90°.

A characteristic of the absorption in a thick slab which appears in Fig. 10 and which is not a consequence of any virtual mode yet discussed is the sharp drop in absorption at low frequency, $\Omega\lesssim\gamma$. There is, in fact, an infinite number of pathological virtual modes lying on the negative Ω axis between 0 and $-i\gamma$, which we would like to relate to this drop at low frequency. To derive the frequencies of these modes we let $\Omega=-i\Omega_2$ in the tangent virtual mode equation (8) and assume that $\gamma\Omega_2\ll\cos\theta$. Then $\beta a=(W/2)[(\gamma/\Omega_2)-1]^{-1/2}$, and Eq. (8) can be written

$$\tan\beta a=[\Omega_2(\gamma-\Omega_2)]^{-1/2}; \tag{42}$$

in a similar way, beginning with the cotangent equation, we get

$$\cot\beta a=-[\Omega_2(\gamma-\Omega_2)]^{-1/2}. \tag{43}$$

The right side of Eqs. (42) and (43) is very large in magnitude since γ is small and Ω_2 is assumed to be small. Therefore $\beta a\approx\frac{1}{2}n\pi$, where $n=2, 4, 6, \cdots$, for the cotangent modes, and $n=1, 3, 5, \cdots$, for the tangent modes, or

$$\Omega_2\approx\frac{\gamma}{1+(W/n\pi)^2}, \tag{44}$$

where n is defined above. Equation (44) applies to P polarization; the result for S polarization is the same except that $n=1, 3, 5, \cdots$ for cotangent modes and $n=2, 4, 6, \cdots$ for tangent modes.

These modes are pathological in the sense that they do not exist when $\gamma=0$: In the limit $\gamma \rightarrow 0$ they all move to the origin of the Ω plane. Therefore Eq. (40) cannot be used to find the contribution of these modes to the absorption. The behavior of L_1 and L_2 along the real Ω axis, which is directly related to the absorption, is in principle determined by the behavior along the imaginary Ω axis, where the zeros of L_1 and L_2 are located. However, a linear expansion of L_1 and L_2 analogous to that used for describing the behavior of these quantities in the neighborhood of an ordinary virtual mode cannot succeed, since many modes are involved and they are far from the real Ω axis in the sense that $\beta a \approx \frac{1}{2}n\pi$ $(n \geq 1)$ at the virtual mode frequencies, while $\beta a \approx 0$ when Ω is on the real axis near $\Omega=0$. We conclude that there is no simple relation analogous to Eq. (40) relating these modes to the absorption near $\Omega=0$.

Some information about the drop in absorption near $\Omega=0$ can nevertheless be obtained by comparing the exact value of the absorption at $\Omega=0$ with the value predicted from the ordinary zero-frequency virtual modes. It can be shown from the exact expressions for the absorption, (37), (38), and (39), that when $\Omega=0$, $A_1=0$ and

$$A=A_2=\frac{4W\gamma\cos\theta}{(W\cos\theta+2\gamma)^2} \tag{45}$$

for P polarization. If $W \ll 1$, the frequency of the $1C_2$ mode is $\eta'+i\eta''=0-i(W/2)\cos\theta$ when $\gamma=0$ and $\rho'+i\rho''=0-i[(W/2)\cos\theta+\gamma]$ when $\gamma \neq 0$. From Eq. (41), the peak absorption at $\Omega=0$ due to the $1C_2$ mode is therefore

$$(A_2)_{\max}=4\gamma/W\cos\theta, \tag{46}$$

which agrees with Eq. (45) if $\gamma \ll W\cos\theta$. This agreement shows that in a thin slab the absorption at $\Omega=0$ is entirely accounted for by the $1C_2$ virtual mode, implying that there cannot be a drop in absorption near $\Omega=0$.[23] For a thick slab, however, the $\Omega=0$ peak occurring when $\theta>45°$ is due to both the $1C_2$ and $0T_2$ modes; the contribution to the absorption from these modes is greater than the exact value at $\Omega=0$, so that near $\Omega=0$ there must be a drop in absorption from the value attributed to the $1C_2$ and $0T_2$ modes to the exact value.

It can be shown similarly for S polarization that when $\Omega=0$, $A_2=0$ and

$$A=A_1=\frac{4W\gamma\cos\theta}{(W+2\gamma\cos\theta)^2}. \tag{47}$$

[23] The numerical calculation shows that the exact absorption at $\Omega=0$ agrees with the peak absorption due to the $1C_2$ mode for $W \lesssim 1$, not only for $W \ll 1$ as the preceding discussion would imply. The other zero-frequency mode $0T_2$ is unimportant for $W \lesssim 1$ since it exists only for θ near 90°, and even when it exists it makes only a small contribution to the absorption.

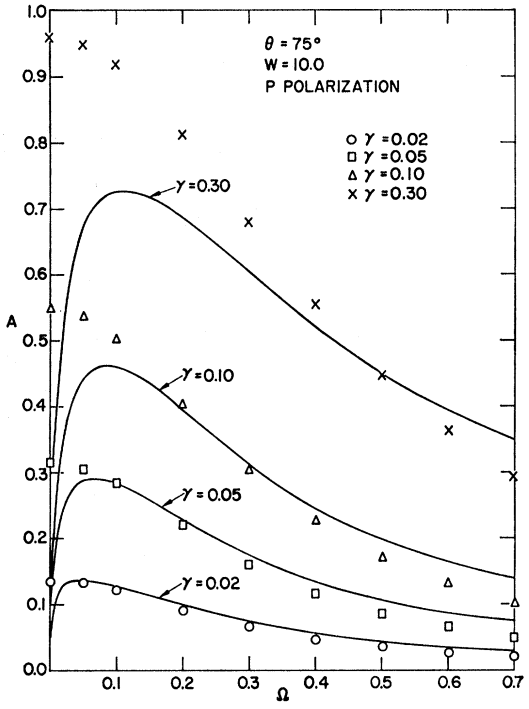

FIG. 11. The low-frequency absorption for a thick crystal and a range of γ. The discrete points are the absorption associated with the $0T_2$ and $1C_2$ modes calculated using Eq. (40). Absorption values obtained from (40) are seen to be below the exact values for frequencies well above the frequency of the mode peak ($\Omega|_{\text{peak}}=0$ for the $0T_2$ and $1C_2$ modes). This is a result of higher-frequency mode contributions appearing in the exact calculation. The subtractive effect associated with those zero-frequency modes which occur for $|\Omega''|<\gamma$ is seen to extend to $\Omega \sim 2\gamma$. For $W \lesssim 10.0$, the transmission of the slab is essentially zero in this frequency range, so the reflection is given by $1-A$, indicating that there is a significant low-frequency reflection dip.

When W is large there are no zero-frequency virtual modes when $\gamma=0$ for S polarization. Therefore the absorption near $\Omega=0$ is small, and there is no interesting peak at or near $\Omega=0$ analogous to that which often occurs for P polarization. When $W=10.0$, for example, the absorption of S-polarized light near $\Omega=0$ at all angles is similar to the absorption of P-polarized light for small angles, as shown in Fig. 10; in particular, no low-frequency peak appears for $\theta>45°$.

If $W>10$, the absorption for $\Omega<1$ is essentially independent of W, except that the sharp drop near $\Omega=0$ changes so that $A=0$ at $\Omega=0$ when $W \rightarrow \infty$, as can be seen from Eqs. (45) or (47). For $\Omega>1$ the peaks which are still distinct at $W=10.0$ move more closely together for larger W and eventually merge into a single structureless absorption peak given for $W \rightarrow \infty$ by setting $\tan\beta a \approx -\cot\beta a \simeq i$ in Eqs. (39).

The absorption spectrum in a thin slab (e.g., $W=0.2$) can easily be adduced by referring to Fig. 7 and Table III. It is evident that the absorption for P polarization is determined by just two modes. The $0T_1$ mode gives a peak at $\Omega \approx 1$ and the $1C_2$ mode, which is better-defined than it is for larger W, gives a peak at $\Omega=0$. The

absorption spectrum for S polarization is even simpler, for only the zero-frequency peak is present.

To this point in the discussion of the optical absorption and its relation to the virtual modes we have taken $\gamma=0.02$. In view of the unique properties of the low-frequency modes, we will briefly examine the low-frequency absorption for a thick crystal when γ is changed. In Fig. 11 are given absorption curves for $W=10.0$, $\theta=75°$, and P polarization. The most interesting feature of these curves is the frequency for which the absorption peaks. For $\gamma\lesssim 0.05$, the peak occurs for $\Omega>\gamma$ ($\Omega|_{\text{peak}}=0.045$ for $\gamma=0.02$), whereas for $\gamma\gtrsim 0.05$, the peak occurs for $\Omega<\gamma$ ($\Omega|_{\text{peak}}=0.110$ for $\gamma=0.30$). The curves of Fig. 11 are essentially unchanged if $W>10.0$, all thickness effects in this range occurring for $\Omega\lesssim 0.05$ [see Eq. (45)].

Reflection and Transmission

It has been pointed out[5] that in most cases, reflection and transmission cannot be readily interpreted in terms of virtual modes because of interference between the modes of opposite parity. Characteristic reflection minima and transmission maxima, only approximately associated with virtual modes, occur for $\Omega>1$ at frequencies such that $\beta a=n\pi/2$. For a thick slab, e.g., $W=10.0$, $T\approx 0$ when $\Omega<1$ and $R\approx 0$ when $\Omega>1$; hence $R\approx 1-A$ for $\Omega<1$ and $T\approx 1-A$ for $\Omega>1$. The absorption peak occurring near $\Omega=0$ for $\theta>45°$ is therefore accompanied by a dip in the reflection. As W decreases, T increases from zero in the range $0<\Omega<1$. The transition from $T\approx 0$ to $T\approx 1$ in this frequency range occurs approximately when the real part of the frequency of the $1C_1$ mode η' moves from $\eta'\gtrsim 1$ to $\eta'=0$, i.e., when $W\approx 1.4$. Therefore if $W\ll 1$, $R\approx 0$ and $T\approx 1$ for most frequencies with the exception of two peaks in R for P polarization (accompanied by minima in T and peaks in A) at $\Omega=0$ and $\Omega\approx 1$ which can be associated quantitatively with the $1C_2$ and $0T_1$ modes, respectively.[24] The sharp dip in T near $\Omega=1$ associated with the $0T_1$ mode provides an accurate means for determining the plasma frequency optically.[18]

V. DISCUSSION

The calculations of the previous section were made considering γ to be independent of frequency, thereby illustrating those aspects of the optical properties dependent on the virtual mode properties *per se*. Since all physical effects contributing to damping must appear in γ because of the form of the dielectric constant used [Eq. (1)], it is clear that in practice γ will depend on the frequency. Assuming $\gamma=\gamma(\Omega)$ [25] does not complicate the formal determination of the virtual modes. That is, a virtual mode calculated using $\epsilon[\Omega,\gamma(\Omega)]$ can still be characterized by a solution $\Omega^c=\rho'+i\rho''$. However, the calculation will still be in effect a constant-γ calculation since the effective γ will be $\gamma(\rho')$. This means that, for a mode essentially isolated from other modes of the same parity, Eq. (41) is still valid if we consider that A need not be $A_{\max}$ but instead becomes $A|_{\rho'}$, i.e., the absorption at the virtual mode frequency. Equation (40) remains valid, however, only in a point-by-point sense. That is, the absorption given by Eq. (40) for $\gamma=\gamma_1$, say, will be a good approximation at only those frequencies for which $\gamma(\Omega)=\gamma_1$. This means, clearly, that a pronounced frequency dependence of γ across a mode will distort severely the Lorentzian line shape. Indeed, peaks can appear at frequencies other than the virtual mode frequencies if γ has the appropriate frequency dependence.

Few general statements can be made concerning the frequency dependence or magnitude of γ for real materials.[26] However, several points of interest in connection with the present discussion should be noted. For energies below those at which interband transitions occur, γ increases significantly with increasing energy for some materials, examples being silver[27] and copper.[28] Materials composed of atoms having similar electronic configurations need not have comparable values of γ. An example is the alkali metals, where the value of γ at the plasma frequency increases significantly with increasing atomic weight, being 0.012 for Na and 0.39 for Cs.[29] The value for Cs indicates that large values of γ do occur. A further illustration of this last remark is the fact that for Ge, in the frequency range where its behavior can be described as free-electron-like, there are indications that γ is as high as 0.40.[30]

A convenient and useful means for including band-structure effects in the dielectric constant for an actual material is to write the dielectric constant, here denoted ϵ', as

$$\epsilon'=\epsilon(\Omega,\gamma)+\delta(\Omega), \tag{48}$$

where $\epsilon(\Omega,\gamma)$ is given by Eq. (1) and $\delta(\Omega)$ is the band contribution. The presence of $\delta(\Omega)$ gives rise to significant effects, one being the displacement of the plasma frequency from the free-electron value. This displacement can be in either direction since band effects of different types can give rise to both positive and negative values of $\delta(\Omega)$.[31] In general, for frequencies greater than the plasma frequency, $\delta(\Omega)$ will be positive corresponding to a core polarization contribution to ϵ'. So, with $\gamma=0$, we have

$$\epsilon'=1-1/\Omega^2+\delta(\Omega), \quad \delta(\Omega)>0, \tag{49}$$

above the plasma frequency.

[24] See Eq. (28) of Ref. 5.

[25] In actual applications where determinations of γ are made, γ is considered to be a function of the real frequency. To remain consistent with such usage, we would consider $\gamma=\gamma(\Omega')$ in the virtual mode calculations.

[26] Recent reviews of work in this area are those of H. Raether, Ref. 14, and J. C. Phillips, Solid State Phys. **18**, 56 (1966).

[27] H. Raether, Ref. 14, p. 128.

[28] H. Raether, Ref. 14, p. 131.

[29] F. Stern, Solid State Phys. **15**, 299 (1963); see p. 345.

[30] N. Swanson, J. Opt. Soc. Am. **54**, 1130 (1964).

[31] H. Raether, Ref. 14, p. 93 ff.

The divergence of Ω' and $|\Omega''|$ for $\theta \to 90°$ in the virtual mode calculations of Sec. III was a consequence of the fact that $\epsilon(\Omega,0) \to 1$ as $\Omega \to \infty$. With a dielectric constant like that of Eq. (49), $\epsilon(\Omega,0)$ can be greater than one for finite frequencies. This results in a radical change in the properties of the virtual modes for large angles; all the modes with $\Omega' \to \infty$ in Sec. III now behave as did the high-frequency virtual modes for an ionic crystal.[2] That is, the virtual modes ($\gamma=0$) now have a finite value of Ω' for $\theta=90°$ with $|\Omega''|$ passing through a maximum (near the Brewster's angle) and becoming 0 for $\theta=90°$. The values of Ω' for $\theta=90°$ are readily obtained, since the tangent equation becomes $\tan\beta a=0$, or $\beta a=\frac{1}{2}n\pi$, n an even integer, whereas the cotangent equation becomes $\cot\beta a=0$, or $\beta a=\frac{1}{2}n\pi$, n an odd integer. Thus the solutions are

$$\Omega'=[\{1+(n\pi/W)^2\}/\delta]^{1/2}. \tag{50}$$

A representative $\Omega>1$ value for δ is 0.2 [32] for which the lowest frequency solution of Eq. (50) is $\Omega'=\sqrt{5}$, independent of crystal thickness. Higher frequency solutions of (50) depend upon the value of W.

The presence of such modes near 90° should be readily detectable since, as $\theta \to 90°$, $|\Omega''|$ calculated with γ included will be $\lesssim\frac{1}{2}\gamma$. Thus, if the crystal is of a thickness such that the modes are separated, an optical experiment with θ near 90° will yield a series of well-defined absorption lines, permitting an accurate high-frequency determination of $\delta(\Omega)$ and $\gamma(\Omega)$.

Since the virtual modes are the collective states of the electron gas which decay radiatively, we expect these modes to appear in the description of radiation which may accompany any mechanism for exciting the system. The use of an electromagnetic wave as a probe was considered in Sec. IV and the radiation spectrum arising from this excitation could be expressed entirely in terms of the virtual modes. In a similar way we can discuss the transition radiation emitted when charged particles pass through the slab.

It will be seen that charged particles constitute a much less selective probe of the virtual modes than an electromagnetic wave. When a wave of frequency ω is incident at an angle θ, the reflection, transmission, and absorption are described in terms of virtual modes characterized by the same angle θ; we can say alternatively that only the virtual modes for the angle θ, with linewidths overlapping the applied frequency, are excited. Furthermore, by suitable polarization of the incident light, S or P modes can be excited selectively. The only selection which cannot be made is to excite modes of a given parity.

In contrast, when charged particles with a given velocity are incident on the slab at a certain angle, the transition radiation is distributed over a continuous range of angles and frequencies. Thus there is no selection of the virtual modes either by frequency or by angle and, in general, S and P modes of both parities are excited. This complete lack of selection in the excitation process is compensated by the fact that the modes can be selected to the same extent as in an optical experiment by suitably analyzing the transition radiation. In this way the angle and frequency can be selected, and the radiation from S- and P-polarized modes can be distinguished by the direction of polarization. Only the radiation from modes of even and odd parity cannot be selected, just as in the case of an optical experiment.

We shall now discuss briefly how the virtual modes enter the mathematical description of transition radiation. In the standard theory of transition radiation[33] it is assumed that the charged particle is essentially undeflected when passing through the slab. The driving fields produced by the charge are taken to be the solutions of the inhomogeneous wave equation both inside and outside the slab, treating each medium as if it were infinite, without any regard to the proper matching of the fields at the surfaces. To these driving fields are added secondary fields which are solutions of the homogeneous wave equation with coefficients determined by the requirements that the total fields satisfy the correct boundary conditions at the surfaces and that the secondary fields outside the slab be outgoing waves. These outgoing waves constitute the transition radiation.

It is found that the Fourier components of the secondary electric field outside the slab have the general form

$$\mathbf{E}(k_x,k_y,\beta_0,\omega)=\mathbf{F}_1{}^p/L_1{}^p+\mathbf{F}_2{}^p/L_2{}^p+\mathbf{F}_1{}^s/L_1{}^s+\mathbf{F}_2{}^s/L_2{}^s, \tag{51}$$

where $L_1{}^p$ and $L_2{}^p$ are the same as L_1 and L_2 in Eq. (39) for P polarization, and $L_1{}^s$ and $L_2{}^s$ are the corresponding quantities for S polarization. The vector functions $\mathbf{F}_1{}^p$, $\mathbf{F}_2{}^p$, $\mathbf{F}_1{}^s$, and $\mathbf{F}_2{}^s$ depend in a complicated way on the particle velocity $\mathbf{v}$, the slab thickness L, the wave-vector components k_x, k_y, β_0, the frequency ω, and the dielectric constant $\epsilon(\omega,\gamma)$. The frequency and the wave vector must obey the restriction $\omega^2=(k_x{}^2+k_y{}^2+\beta_0{}^2)c^2$. The secondary magnetic field can also be written in the form given by Eq. (51). The Poynting vector is in the direction of the wave vector and is of the form

$$\mathbf{S}=\mathbf{S}^p+\mathbf{S}^s, \tag{52}$$

where

$$\mathbf{S}^p=\mathbf{G}_1{}^p/|L_1{}^p|^2+\mathbf{G}_{12}{}^p/|L_1{}^pL_2{}^{*p}|+\mathbf{G}_2{}^p/|L_2{}^p|^2$$

and

$$\mathbf{S}^s=\mathbf{G}_1{}^s/|L_1{}^s|^2+\mathbf{G}_{12}{}^s/|L_1{}^sL_2{}^{*s}|+\mathbf{G}_2{}^s/|L_2{}^s|^2,$$

[32] E. T. Arakawa, R. N. Hamm, W. F. Hanson, and T. M. Jelinek, in *Optical Properties and Electronic Structure of Metals and Alloys*, edited by F. Abeles (North-Holland Publishing Company, Amsterdam, 1966), p. 374.

[33] R. H. Ritchie and H. B. Eldridge, Phys. Rev. **126**, 1935 (1962). A review of the Russian literature on transition radiation is given by F. G. Bass and V. M. Yakovenko, Usp. Fiz. Nauk **86**, 189 (1965) [English transl.: Soviet Phys.—Uspeki **8**, 420 (1965)].

where the G functions are related to the F functions of Eq. (51). The appearance of the L functions in the denominators means that, just as for the optical properties, there are, in general, peaks in the transition radiation spectrum at frequencies corresponding to the virtual mode frequencies. However, the interference term containing $|L_1L_2^*|$ has the consequence that when modes of opposite parity overlap, one of them may be associated with a minimum in the radiated power, rather than a maximum. In this respect transition radiation is analogous to reflectance and transmittance in an optical experiment, which also contain interference terms between modes of opposite parity. The quantities G in Eq. (52) are sufficiently complicated functions of the frequency that they can introduce additional structure into the power spectrum. In an optical experiment, on the other hand, essentially all structure can be attributed to the virtual modes.

For the special case of normally incident particles, only P-polarized modes are excited, i.e., $\mathbf{F}_1^s=\mathbf{F}_2^s=0$ in Eq. (51) or $\mathbf{S}^s=0$ in Eq. (52). This is evident physically since the magnetic field associated with the incident particle is parallel to the slab, as is the magnetic field accompanying the P-polarized modes. For obliquely incident particles, including an angle of 90°, both S- and P-polarized modes are excited.

A brief discussion of the surface plasmons was given in Sec. II. Recent work in connection with the excitation of such modes by electrons warrants a few additional comments. If retardation is neglected, the surface mode equations [(2) and (6)] become

$$\Omega^2=\tfrac{1}{2}(1\pm e^{-k_xL}). \tag{53}$$

Takimoto[34] has investigated the energy loss of a fast electron moving parallel to the surface of a metallic slab in a calculation in which retardation is neglected. Assuming specular reflection of the electrons at the surface, he finds that, for a thick slab ($k_xL\gg1$),[35] energy extraction from the moving electron occurs at $\Omega^2=\frac{1}{2}$, which is the surface mode frequency of Eq. (53) in this limit. For a thin slab ($k_xL\ll1$) and specular reflection he finds the energy extraction occurring at $\Omega^2=\frac{1}{2}k_xL$, which is the low-frequency solution of (53) when $k_xL\ll1$, again indicating that a surface mode is being excited by the electrons. A puzzling feature of this result is, if surface modes are indeed being excited, and there is every indication they are, why does the high-frequency surface mode not share in the excitation? In fact it does, for if one evaluates the general expression for the force on the electron given by Takimoto,[36] the energy delta-function has the form

$$\delta[\Omega^2-\tfrac{1}{2}(1\pm e^{-k_xL})],$$

which means that the excitation frequencies are just those of Eq. (53). Thus the force expression given by Takimoto for the case of a thin crystal is incomplete, the correct conclusion being that the passage of the electron does excite both surface modes. This is a most interesting conclusion, particularly in view of the recent studies of Boersch *et al.*[37] suggesting that the surface modes excited by electrons rather surprisingly radiate.[38] It should be emphasized that the calculation of Takimoto does not include retardation effects, which will have a marked effect on the conclusions for a thin crystal.

Takimoto concludes further that, for the case of diffuse surface electron scattering and an infinite crystal, the surface plasmon peak is no longer sharp, but is broadened about $\Omega=1/\sqrt{2}$. This points up one fact concerning the present work. The consequences of including the anomalous skin effect in the calculations of the present paper have not been explored. These effects should be investigated.

[34] N. Takimoto, Phys. Rev. **146**, 366 (1966).

[35] k_x and L in the present case correspond to q and d in Ref. 34. This corresponds physically to the requirement that the plasma frequency times the time necessary for the electron to move a distance equal to the crystal thickness be large compared to one.

[36] This is given by the bottom equation in the left-hand column of p. 370 of Ref. 34.

[37] H. Boersch, P. Dobberstein, D. Fritzsche, and G. Sauerbrey, Z. Physik **187**, 97 (1965).

[38] A reservation concerning the interpretation of the observed radiation as being due to radiative decay of surface plasmons has been expressed by L. S. Cram, E. T. Arakawa, and R. D. Birkhoff, Bull. Am. Phys. Soc. **11**, 364 (1966).